Optics Communications 413 (2018) 276–282

Contents lists available at ScienceDirect

Optics Communications

journal homepage: www.elsevier.com/locate/optcom

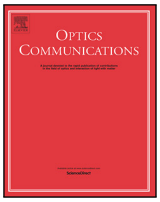

All-fiber probe for optical coherence tomography with an extended depth of focus by a high-efficient fiber-based filter

Jianrong Qiu, Yi Shen, Ziwei Shangguan, Wen Bao, Shanshan Yang, Peng Li, Zhihua Ding *

College of Optical Science and Engineering, State Key Lab of Modern Optical Instrumentation, Zhejiang University, Hangzhou 310027, China

ARTICLE INFO

Keywords:
Fiber-based filter
Depth of focus extension
Beam propagation method
Optical coherence tomography

ABSTRACT

Although methods have been proposed to maintain high transverse resolution over an increased depth range, it is not straightforward to scale down the bulk-optic solutions to minimized probes of optical coherence tomography (OCT). In this paper, we propose a high-efficient fiber-based filter in an all-fiber OCT probe to realize an extended depth of focus (DOF) while maintaining a high transverse resolution. Mode interference in the probe is exploited to modulate the complex field with controllable radial distribution. The principle of DOF extension by the fiber-based filter is theoretically analyzed. Numerical simulations are conducted to evaluate the performances of the designed probes. A DOF extension ratio of 2.6 over conventional Gaussian beam is obtainable in one proposed probe under a focused beam diameter of $4.6\ \mu\text{m}$. Coupling efficiencies of internal interfaces of the proposed probe are below −40 dB except the last probe–air interface, which can also be depressed to be −44 dB after minor modification in lengths for the filter. Length tolerance of the proposed probe is determined to be $-28/+20\ \mu\text{m}$, which is readily satisfied in fabrication. With the merits of extended-DOF, high-resolution, high-efficiency and easy-fabrication, the proposed probe is promising in endoscopic applications.

1. Introduction

Optical coherence tomography (OCT) is an attractive imaging modality due to its ability to acquire in vivo high-resolution structural or/and functional information of biological tissues using minimized probes [1]. Imaging of biomedical tissues with high resolution over an extended depth range is increasingly significant both in biological research and medical practice [2]. In contrast to conventional optical imaging systems, axial resolutions in OCT are decoupled from their lateral resolutions and primarily determined by the coherence length of the adopted light sources. Using the state-of-the-art broadband light sources, axial resolutions of a few micrometers have been demonstrated [3]. However, it is not straightforward to increase their transverse resolutions to similar values without severely compromising the useful depth range. Due to inverse proportional relationship of the depth of focus (DOF) with the square of the numerical-aperture (NA) of the focusing objective, a tradeoff between the transverse resolution and the depth of focus (DOF) has to be made.

To resolve this dilemma, extensive investigations have been conducted to maintain high transverse resolution over an increased depth range, those include numerical refocusing [4], depth-encoded synthetic aperture [5,6], dynamic focusing [7], multi-beam [8,9], quasi-Bessel beam [10–13] and aperture apodization [14–16]. Among them, algorithms used for numerical refocusing are computational intensive and demanding on phase stability. The method of depth-encoded synthetic aperture also requires phase stability, and its implementation in a miniature probe is difficult if not impossible. Dynamic focusing is successful in time domain OCT, but not well suitable for Fourier domain OCT where information for whole depth range is fetched simultaneously. Approach based on multi-beam requires parallel acquisition at different focal depths to achieve an extended DOF. However, the complexity of the system is increased and realignment of sub-images is needed [9]. Approach based on quasi-Bessel beam can achieve enough DOF for most applications, but suffered from artifacts due to side lobes and degraded light efficiency. Decoupling the illumination path from the detection path was proposed to improve the light efficiency [12]. However, scaling down this bulk-optic solution to minimized probe is difficult. Aperture apodization such as using an annular apodization [14], a phase filter [15], or a complex filter [16] on the aperture of the focusing objective is a well-exploited method to extend the DOF. Annular apodization has been intensively researched in imaging engineering [14]. One shortcoming of this approach is the reduced light transmission efficiency due to central obstruction. Consequently, binary phase spatial filter

---

* Corresponding author.
E-mail address: zh_ding@zju.edu.cn (Z. Ding).

https://doi.org/10.1016/j.optcom.2017.12.048
Received 24 September 2017; Received in revised form 22 November 2017; Accepted 17 December 2017

(BPSF) was proposed to enhance the light transmission efficiency [15], and complex filter was introduced for the optimization of light energy within the DOF region [16]. However, to implement these approaches based on phase filter or complex filter to minimized probes, one must face the challenges in filter fabrication and optical alignment. Although a feasible study was conducted to stamp a BPSF onto the end of a minimized probe [15], the required filter demands dedicated fabrication and careful alignment. Alternatively, a fiber-based phase mask was demonstrated with a precisely controlled short section of graded index fiber (GIF). However, the strict tolerance (~4 μm) in length control of the GIF crucial to probe performance increases the difficulty in probe fabrication [17].

In this paper, we propose a high-efficient fiber-based filter in an all-fiber OCT probe to realize an extended DOF while maintaining a high transverse resolution. The filter is consisted by a section of graded index fiber (GIF) and a section of large core fiber (LCF). The GIF of the filter is introduced to enhance light transmission efficiency and manipulate the excited modes to the LCF. Mode interference in the probe is exploited to modulate the complex field. The field exiting from the filter is controllable by varied fiber lengths for the filter. Complex field with the expected radial distribution can be realized on the aperture of the objective to extend the DOF. Due to all-fiber configuration of the proposed OCT probe, difficulties in filter fabrication and component alignment are greatly reduced.

The paper is organized as follows. Firstly, the principle of DOF extension by the fiber-based filter is introduced. Then, numerical simulations on the performance of the proposed probes as well as the conventional probe are presented. Finally, the conclusion is drawn.

2. Principle of DOF extension by the fiber-based filter

As shown in Fig. 1(a), a typical all-fiber OCT probe is consisted by a section of single mode fiber (SMF) for light delivery, a section of no core fiber (NCF) for beam expansion and a section of GIF (labeled as GIF2) as an objective for beam focusing. To extend the DOF, the GIF–LCF based filter is added in the proposed all-fiber OCT probe as shown in Fig. 1(b). The GIF (labeled as GIF1) in the filter is introduced to enhance light transmission efficiency and manipulate the excited modes to the following LCF. By varying lengths for the GIF1 and the LCF, controllable fields at the interface of LCF–NCF can be resulted. Providing the fiber specifications in Table 1, the annular profile giving best performance in DOF extension is depicted in Fig. 1(b), which resembles to the annular apodization frequently adopted to extend the DOF [18]. It is noteworthy that this annular apodization is formed by interference of the guided modes instead of central obstruction or an appended filter.

When the proposed OCT probe shown in Fig. 1(b) is interfaced with an OCT system, the light from the source is delivered to the OCT probe via the SMF. Modeling the exiting beam from the SMF at the interface of SMF–GIF1 by a Gaussian beam with complex beam parameter $q_{\mathrm{SMF}} = i n_{\mathrm{SMF}} k_0 w_{\mathrm{SMF}}^2/2$, where n_{SMF} is the core refractive index of SMF, k_0 is the center wavenumber of the light source in free space, and w_{SMF} is the waist radius defined by half mode field diameter (MFD) of the SMF, then the complex beam parameter q_{GIF1} at the interface of GIF1–LCF can be approximated by the following ABCD matrix formulation [19,20]:

$$q_{\mathrm{GIF1}} = \frac{\cos(gL_{\mathrm{GIF1}})q_{\mathrm{SMF}} + \frac{n_{\mathrm{SMF}}}{n_{\mathrm{GIF1}}g}\sin(gL_{\mathrm{GIF1}})}{-\frac{n_{\mathrm{GIF1}}}{n_{\mathrm{LCF}}}g\sin(gL_{\mathrm{GIF1}})q_{\mathrm{SMF}} + \frac{n_{\mathrm{SMF}}}{n_{\mathrm{LCF}}}\cos(gL_{\mathrm{GIF1}})}, \tag{1}$$

where g and L_{GIF1} are the gradient constant and the length of the GIF1 respectively, n_{GIF1} is the refractive index of GIF1 on fiber axis, and n_{LCF} is the core refractive index of LCF. The field at the interface of GIF1–LCF is then given by

$$E_{\mathrm{GIF1}}(r) = \frac{A}{q_{\mathrm{GIF1}}}\exp\left[-in_{\mathrm{GIF1}}k_0\frac{r^2}{2q_{\mathrm{GIF1}}} - in_{\mathrm{GIF1}}k_0L_{\mathrm{GIF1}}\right]. \tag{2}$$

Here r is the radial coordinate, and A represents amplitude constant. It is noted that the time dependent part $\exp(i\omega t)$ is not explicitly shown for brevity. This field expressed by Eq. (2) can be recognized as series of linearly polarized (LP) modes in the following LCF. Among these LP modes, only LP_{0n} modes with zero angular momenta are excited, due to cylindrical symmetry of the fibers and the assumed perfect angular and lateral alignment at spliced interfaces. Thus, by adding the radiation field corresponding to coupling loss, Eq. (2) can be rewritten as

$$E_{\mathrm{GIF1}}(r) = \sum_{n=1}^{N} c_n\psi_n(r) + \text{radiation field}, \tag{3}$$

where N is the number of finite LP_{0n} mode supported in the LCF, and $\psi_n(r)$ is the mode field which can be expressed as follow,

$$\psi_n(r) = \begin{cases} J_0(r\sqrt{k_0^2n_{\mathrm{LCF}}^2 - \beta_n^2}) & r \le \rho \\ b_nK_0(r\sqrt{\beta_n^2 - k_0^2n_{\mathrm{cl}}^2}) & r > \rho. \end{cases} \tag{4}$$

Here J_0 and K_0 represent the 0th-order Bessel function and the 0th-order modified Bessel function of the second kind, and b_n is a constant satisfying $b_n = \frac{J_0(\rho\sqrt{k_0^2n_{\mathrm{LCF}}^2-\beta_n^2})}{K_0(\rho\sqrt{\beta_n^2-k_0^2n_{\mathrm{cl}}^2})}$. ρ and n_{cl} are the core radius and the cladding refractive index of the LCF. β_n is the propagation constant of LP_{0n} mode. The mode excitation coefficient c_n in Eq. (3) can be estimated according to mode orthogonality:

$$c_n = |c_n|\exp(i\phi_{0n}) = \frac{\int_0^\infty E_{\mathrm{GIF1}}(r)\psi_n^*(r)r\,\mathrm{d}r}{\int_0^\infty |\psi_n(r)|^2r\,\mathrm{d}r}, \tag{5}$$

where $|c_n|$ and ϕ_{0n} denote mode excitation amplitude and phase at the interface of GIF1–LCF, respectively, and the star (*) represents complex conjugate. Using overlap integral in radial coordinates and normalizing the mode power to the input power, the mode power coupling efficiency η_n related to $|c_n|$ can be estimated by

$$\eta_n = |c_n|^2\frac{\int_0^\infty |\psi_n(r)|^2r\,\mathrm{d}r}{\int_0^\infty |E_{\mathrm{GIF1}}(r)|^2r\,\mathrm{d}r}. \tag{6}$$

Since the structure is uniform along the fiber axis, the field propagation in LCF can be described in terms of modes $\psi_n(r)$ with different β_n. Combining Eqs. (3), (5), (6) and neglecting the radiation field, the field at the interface of LCF–NCF after propagating through LCF with a length of L_{LCF} can be expressed by

$$\begin{aligned} E_{\mathrm{LCF}}(r) &= \sqrt{\int_0^\infty |E_{\mathrm{GIF1}}(r)|^2r\,\mathrm{d}r}\sum_{n=1}^{N}\sqrt{\eta_n}\frac{\psi_n(r)}{\sqrt{\int_0^\infty |\psi_n(r)|^2r\,\mathrm{d}r}} \\ &\quad \times \exp(i\phi_{0n} + i\beta_nL_{\mathrm{LCF}}). \end{aligned} \tag{7}$$

It is observed from Eq. (7) that the field at the interface of LCF–NCF is resulted from coherence superposition of guided modes whose coupling efficiencies and phases are controllable by fiber lengths of the filter. After propagation of the field in the following NCF, the expected field acting as the complex filter to extend the DOF is generated on the aperture of the GIF2, the focusing objective of the all-fiber OCT probe.

3. Numerical simulations on the performance of the OCT probe

In principle, it is feasible to provide an estimation of the performance of the designed probe using Eqs. (1)–(7). However, for comprehensive description of the field and better evaluation of the performance, numerical simulations on the designed probes using the radial beam propagation method (BPM) are conducted. Specifications of the adopted fibers in the proposed all-fiber OCT probe are listed in Table 1. The probe is assumed to be immersed in air with refractive index of 1 under the light source with center wavelength of 1.3 μm. Transversal grid size and longitudinal step size in the simulations are set to be 0.1 μm and 1 μm, respectively.

In consideration of the limited V-number of 6.04 for the LCF, it is determined that only two modes (LP_{01} and LP_{02}) are allowable in the proposed all-fiber OCT probe. Therefore, numerical simulations on